Development 134, 2627-2638 (2007) doi:10.1242/dev.005611

Cellular dynamics associated with the genome-wide epigenetic reprogramming in migrating primordial germ cells in mice

Yoshiyuki Seki[1], Masashi Yamaji[1,2], Yukihiro Yabuta[1], Mitsue Sano[1,3], Mayo Shigeta[1], Yasuhisa Matsui[4], Yumiko Saga[5], Makoto Tachibana[6], Yoichi Shinkai[6] and Mitinori Saitou[1,2,7,*]

We previously reported that primordial germ cells (PGCs) in mice erase genome-wide DNA methylation and histone H3 lysine9 di-methylation (H3K9me2), and instead acquire high levels of tri-methylation of H3K27 (H3K27me3) during their migration, a process that might be crucial for the re-establishment of potential totipotency in the germline. We here explored a cellular dynamics associated with this epigenetic reprogramming. We found that PGCs undergo erasure of H3K9me2 and upregulation of H3K27me3 in a progressive, cell-by-cell manner, presumably depending on their developmental maturation. Before or concomitant with the onset of H3K9 demethylation, PGCs entered the G2 arrest of the cell cycle, which apparently persisted until they acquired high H3K27me3 levels. Interestingly, PGCs exhibited repression of RNA polymerase II-dependent transcription, which began after the onset of H3K9me2 reduction in the G2 phase and tapered off after the acquisition of high-level H3K27me3. The epigenetic reprogramming and transcriptional quiescence were independent from the function of Nanos3. We found that before H3K9 demethylation, PGCs exclusively repress an essential histone methyltransferase, GLP, without specifically upregulating histone demethylases. We suggest the possibility that active repression of an essential enzyme and subsequent unique cellular dynamics ensures successful implementation of genome-wide epigenetic reprogramming in migrating PGCs.

KEY WORDS: Primordial germ cells (PGCs), Histone modifications, Reprogramming, Cell cycle, Epigenetics, Mouse

INTRODUCTION

In the development of multicellular organisms, the genome of a single fertilized oocyte generates diverse cell types with distinct gene expression profiles. The differentiated cells generally maintain their gene expression through epigenetic mechanisms, including DNA methylation (Bird, 2002) and covalent modifications of histone N-terminal tails (Martin and Zhang, 2005; Peters and Schubeler, 2005), which are often mitotically heritable. Thus, each cell type in our body acquires a specific and stable epigenetic signature, often referred to as 'cellular memory'. The genome of the germ cell lineage, the sole source for the next generation, however, must be maintained in an epigenetically 'reprogrammable' state in order for the creation of new generations to continue. Therefore, the germline, from its outset, must be endowed with a certain mechanism to ensure this crucial function.

There are essentially two modes, which are known as 'preformation' and 'epigenesis', respectively, for the specification of germ cell fate during the development of multicellular organisms (Extavour and Akam, 2003). The preformation, which is seen in model organisms such as *Caenorhabditis elegans* and *Drosophila melanogaster*, involves localized maternal determinants present in the egg, often referred to as the germ plasm, for the specification of germ cell fate. The molecular components of the germ plasm and the epigenetic properties of the early germline cells that inherit it have been analyzed, leading to a general concept that the germ plasm imposes transient yet robust transcriptional quiescence on the genome at the outset of the germ cell lineage with appropriate epigenetic modifications (Seydoux and Braun, 2006).

By contrast, in the 'epigenesis', which is seen in many organisms, including mammals, a potentially equivalent population of cells at a relatively late stage of development is induced to form either germ cells or somatic mesoderm in response to signaling molecules from adjacent tissues (Lawson et al., 1999; McLaren, 2003; Ohinata et al., 2006). This implies that cells recruited for the germline may have to undergo 'epigenetic reprogramming' from a somatic to a potentially totipotent germline phenotype. Blimp1 (Prdm1 – Mouse Genome Informatics), a potent transcriptional repressor with a PR domain and five zinc fingers, which is initially expressed in a few cells of the most proximal epiblast cells at embryonic day (E) 6.25, has been identified as a crucial requirement for the birth of this lineage (Ohinata et al., 2005). *Blimp1*-positive lineage-restricted precursors of PGCs increase in number and exclusively go on to form stella (*Pgc7*, *Dppa3*)-positive founder PGCs at around E7.25 that repress the somatic mesodermal program, including Hox gene expression, and reactivate the pluripotency-associated gene network (Ohinata et al., 2005; Saitou et al., 2002; Sato et al., 2002; Yabuta et al., 2006). Subsequently, from around E7.5 onwards, these cells initiate the migration towards future genital ridges through the visceral and definitive hindgut endoderm.

[1]Laboratory for Mammalian Germ Cell Biology, Center for Developmental Biology, RIKEN Kobe Institute, 2-2-3 Minatojima-Minamimachi, Chuo-ku, Kobe, 650-0047, Japan. [2]Laboratory of Molecular Cell Biology and Development, Graduate School of Biostudies, Kyoto University, Oiwake-cho, Kitashirakawa, Sakyo-ku, Kyoto 606-8502, Japan. [3]Department of Biosystems Science, Graduate School of Science and Technology, Kobe University, 1-1 Rokkodai-cho, Nada-ku, Kobe 657-8501, Japan. [4]Cell Resource Center for Biomedical Research, Institute of Development, Aging and Cancer, Tohoku University, 4-1 Seiryo-cho, Aoba-ku, Sendai 980-8575, Japan. [5]Department of Genetics and Division of Mammalian Development, National Institute of Genetics, SOKENDAI, 1111 Yata, Mishima, Shizuoka 411-8540, Japan. [6]Department of Cell Biology, Institute for Virus Research, Kyoto University, Shogoin Kawara-cho, Kyoto 606-8507, Japan. [7]Precursory Research for Embryonic Science and Technology, Japan Science and Technology Agency, 4-1-8 Hon-cho, Kawaguchi, Saitama 332-0012, Japan.

*Author for correspondence (e-mail: saitou@cdb.riken.jp)

Accepted 10 May 2007

There has been a dearth of information and investigation on what is happening at the cellular and molecular levels in the migrating PGCs, although it has been established that PGCs undergo extensive epigenetic reprogramming, including erasure of parental imprints and reactivation of inactive X chromosome, when they colonize the genital ridges (Li, 2002; McLaren, 2003; Surani, 2001). Our previous study demonstrated that PGCs have already initiated a genome-wide epigenetic reprogramming in their migration period (Seki et al., 2005); they undergo a significant loss of both DNA methylation and H3K9me2, two repressive modifications with higher stability, from their genome at around E8.0 and instead acquire high levels of H3K27me3, another repressive modification with apparent plasticity, at around E9.0, suggesting that this reprogramming might be essential for the potential totipotency of PGCs. However, the mechanisms of this epigenetic reprogramming are unclear, and their clarification could provide essential information on the reprogramming of somatic cell nuclei generally. In this report, we provide a precise analysis of the cellular dynamics associated with the epigenetic reprogramming in migrating PGCs.

MATERIALS AND METHODS

Antibodies

The following antibodies were used at the indicated dilution and obtained from the indicated sources: rat anti-GFP (1/500, Nacalai 04404-26); rat anti-HA (1/50, Roche); rabbit anti-H3K9me1 (1/500, Upstate 07-450); rabbit anti-H3K9me2 (1/500, Upstate 07-441); rabbit anti-H3K9me3 (1/500, Upstate 07-442); rabbit anti-H3K27me2 (1/500, Upstate); rabbit anti-H3K27me3 (1/500, Upstate 07449); rabbit anti-H3K4me2 (1/500, 07-030); rabbit anti-H3K4me3 (1/500, Upstate 07-473); mouse anti-phospho-pol II (H5, 1/100, Covance Research MMS-129R; H14, 1/100, Covance Research MMS-134R); rabbit anti-pol II (1/100, Santa Cruz sc-899); mouse anti-BrdU (1/100, Roche); mouse anti-cyclin B1 (1/50, Santa Cruz sc-245); mouse anti-SSEA1 (1/100, Hybridoma Bank, University of Iowa) and mouse GLP and G9a antibodies as described previously (Tachibana et al., 2002; Tachibana et al., 2005). The rabbit anti-stella antibody was generated by GST fusion of the N-terminal half of stella as an antigen, affinity-purified, and used at a dilution of 1:1000.

The following secondary antibodies from Molecular Probes were used at a 1/500 dilution: Alexa Fluor 488 goat anti-rat IgG; Alexa Fluor 488 anti-rabbit IgG; Alexa Fluor 568 anti-rabbit IgG; Alexa Fluor 568 anti-mouse IgG; Alexa Fluor 568 anti-mouse IgM; and Alexa Fluor 633 anti-rabbit IgG.

Embryo isolation and staging

All the animals were treated with appropriate care according to the RIKEN ethics guidelines. Embryos were isolated in Dulbecco's Modified Eagle's Medium (DMEM) (Invitrogen) supplemented with 10% FCS (Stem Cell Science). Noon of the day when the vaginal plugs of mated females were identified was scored as E0.5. For a more accurate staging, embryos younger than E8.0 were classified according to the morphological landmarks (Downs and Davies, 1993), and we corresponded embryonic days to embryonic stages as follows: E6.5, early streak (ES); E6.75, mid streak (MS); E7.0, late streak (LS); E7.25, early bud (EB); E7.5, late bud (LB); E7.75, early head fold (EHF); E8.0, late head fold (LHF). Embryos older than E8.25 were staged according to the somite numbers (St) as follows: E8.25, 2-4 St; E8.5, 6-8 St; E8.75, 10-12 St; E9.0, 14-16 St; E9.25, 18-20 St; E9.5, 22-24 St; E9.75, 26-28 St; E10.0, 30-32 St; E10.25, 34-36 St; E10.5, 38-40 St.

Transgenic animals and *Nanos3* knockout mice

Blimp1-mEGFP transgenic mice were generated as described previously (Ohinata et al., 2005), and backcrossed to C57Bl/6 background at least five times. stella-EGFP transgenic mice on a C57Bl/6 background were generated by pronuclear injection of a bacterial artificial chromosome bearing the stella locus with the *EGFP* sequence fused to the end of the stella sequence (Payer et al., 2006) (a kind gift of Dr M. Azim Surani, Gurdon Institute, Cambridge, UK). *Nanos3* knockout mice (Tsuda et al., 2003) were maintained on a C57Bl/6/DBA background.

Whole-mount immunohistochemistry and confocal microscopic analyses

Female CD1 mice were mated with male *Blimp1*-mEGFP or stella-EGFP transgenic lines, and were sacrificed at the appropriate stages to recover embryos. Embryonic fragments from extra-embryonic mesoderm (E7.0), the base of allantois (E7.25-8.0), hindgut epithelium (E8.25-9.25), hindgut epithelium and mesentery (E9.5-10.0), and urogenital ridges (E10.25-10.5) were dissected out and cut into smaller pieces to facilitate antibody permeabilization. They were washed with PBS containing 0.1% BSA, fixed in 4% paraformaldehyde (PFA) in PBS at 4°C for 30 minutes and subjected to three 15 minute washes with PBS containing 1% Triton-X (PBS-T). The fragments were incubated with primary antibodies in PBS-T containing 1 mg/ml BSA for 4 days at 4°C, washed with PBS-T, incubated with the Alexa Fluor secondary antibodies in PBS-T containing 1 mg/ml BSA and 1 μg/ml Hoechst 33342 for 2 days at 4°C, washed with PBS-Triton, mounted in Vectashield (Vector Laboratories) and observed under a confocal microscope (Zeiss or Olympus). Immunofluorescence images were acquired through the *z*-axis of the fragments at an interval of 4 μm.

PGC counts

To count the PGC number, *Blimp1*-mEGFP and stella-EGFP transgenic embryos (C57Bl/6/CD1 F1) were used for E7.0-7.75 and for E8.0-10.5, respectively. Embryonic fragments were collected as described above and used for immunofluorescence staining with the anti-GFP antibody. All the fragments were processed for confocal analysis as described above.

BrdU labeling

We used a BrdU labeling and detection Kit (Roche) for analyzing the incorporation of Bromo-deoxyuridine (BrdU) into PGCs. Pregnant females mated either with *Blimp1*-mEGFP or stella-EGFP males were injected intraperitoneally with BrdU (10 mg/kg body weight) at appropriate stages. After 6 hours, the embryos were isolated and fragments containing PGCs were dissected out, cut into smaller pieces, fixed with 70% EtOH in 50 mM glycine for 4 hours and washed in PBS. These pieces were incubated with anti-BrdU and anti-GFP antibodies in incubation buffer at 37°C for 3 hours, washed with PBS, incubated with the Alexa Fluor 568 secondary antibodies in PBS containing 1 μg/ml Hoechst 33342 at 4°C for 2 hours, and then washed again with PBS, mounted in Vectashield and observed under a confocal microscope.

BrUTP labeling

At E8.75, hindgut epithelia containing PGCs were isolated, incubated with 0.25% trypsin, 0.5 mM EDTA in PBS for 10 minutes and dissociated into single cells by pipetting. Dissociated cells were allowed to adhere to slides by incubating in DMEM supplemented with 10% FCS at room temperature for 20 minutes. Cells were then incubated with Tris-glycerol buffer [20 mM Tris-HCl, pH 7.4, 5 mM $MgCl_2$, 25% glycerol, 0.5 mM phenyl-methylsulphonylfluoride (PMSF), 2 mM 4-(2-aminoethyl) benzenesulfonyl fluoride hydrochloride (AEBSF)], permeabilized in the same buffer with 5 μg/ml digitonin at room temperature for 3 minutes, and then incubated with transcription buffer [50 mM Tris-HCl, pH 7.4, 10 mM $MgCl_2$, 0.5 mM EGTA, 100 mM KCl, 25% glycerol, 0.025 mM S-adenosyl methionine, 0.75 mM BrUTP, 0.5 mM PMSF, 25 U/ml (1 μl) RNasin, 0.5 mM each nucleotide triphosphate, 4 mM AEBSF] for 30 minutes at 37°C. At the end of the transcription reaction, cells were gently rinsed with PBS, fixed in 4% paraformaldehyde in PBS and processed for immunofluorescence staining with anti-BrUTP and stella antibodies.

Fluorescence-activated cell sorting (FACS) analysis

Embryonic fragments containing PGCs of E7.25 *Blimp1*-mEGFP (visceral endoderm removed), E7.75, 8.25, 8.75, 9.75 and 10.5 stella-EGFP transgenic embryos were dispersed into single cells by incubating with 0.25% trypsin, 0.5 mM EDTA in PBS and fixed with 3.7% PFA in PBS at 4°C for 30 minutes. Cells were collected by centrifugation (3000 rpm, 5 minutes), washed in PBS containing 1% BSA, incubated with 50 μg/ml propidium iodide (Molecular Probes), 0.005% saponin (SIGMA) and 0.25 mg/ml RNase A at 37°C for 20 minutes and immediately analyzed on a flow cytometer (FACS Canto; Becton Dickinson). In total, over 10,000 events were collected and gated through doublet discrimination to analyze the DNA

Table 1. Primer sequences of the JmjC domain-containing genes

Gene	Accession No.	Primer 1	Primer 2	Amplicon (bp)
1110034B05Rik	NM_001037742	TGTGCAGATCTTGGACAGAGC	TTCTTGCTGTAGGCTTTGTCTTG	114
2410016O06Rik (*No66*)	NM_023633	GAGACATTGGGGGTTTTATATGG	ATACAAACTTAACGCGCAGCAC	100
2610003J06Rik	NM_028101	ACACTCCTCCAGTTCCCTGAG	AGGACAACAACCGGTACATGG	127
A630082K20Rik (*KIAA1718*)	NM_001033430	TGCTAACATCCAAGGTGCATAC	TGAACATGTTTCCCTGCAAAG	126
Fbxl10 (*Jhdm1b*)	NM_001003953	ACCTCTCCCTCAGACTTGAGC	AGGGTGTGGGCACATTTATTC	124
Fbxl11 (*Jhdm1a*)	NM_001001984	TTGGAAGTGTGTGTGCATGTG	CGTTCAATGCAAAGTCAAAGG	147
Hif1an (*Fih1*)	NM_176958	TCTGGTCCCTTTGGTACATTTC	CCACCCCCACAAGTCATTATAG	112
Hr	NM_021877	ACTGCTTTTGCCTTCCTACCTC	AAAAATCCCCAAACCACAGC	101
Hspbap1	NM_175111	AAGTACTCTGGCTCTGCATGG	AACACCACGTGGGTATGTGAG	102
Jarid1a	XM_359326	GCTGAATAAATTGGCCAAGAAG	TCTTCTCCGTGCTCTCTTTCAC	107
Jarid1b	NM_152895	GCACCAAGCCGAAAGTAAAAAC	CCAGTCCTGTAGCTTTGCTGAG	100
Jarid1c	NM_013668	TTTTCCCTTCCCCTTACTGTTC	CCAAAAGCCTTCAGACCATAGG	123
Jarid1d	NM_011419	CCATCAATATTCCTGGGACTAGC	GTTTTGATGTGTGATTGATGAAGG	144
Jarid2	NM_021878	TGATGTACCGCTACGATGAGG	TTGGTGTGGGTTTGTTGAGAC	111
Jmjd1a (*Jhdm2a*)	NM_173001	CGTCTGGACAGCTCATTCAAG	CACTTCCTCCATTGCTCTTCTG	131
Jmjd1b (*Jhdm2b*)	XM_619530	ACTCCTCATGTGTGTCCAAACG	AAAACTCCACTGAGTTGGAAAGC	123
Jmjd1c (*Jhdm2c*)	XM_907708	TCTCATTTTGGTAAAATTTATGTGAAG	TTGCACTTTAACAAAAGCAAGC	131
Jmjd2a	NM_172382	ACAGGTTCCTGAATTTGTTTGC	ACAAGGTAATGCACCGGTTTTC	150
Jmjd2b	NM_172132	GAGAGGTCCGGGTTTTTGTG	GATACTGAACTGGAGGCCAGAG	109
Jmjd2c	NM_144787	TTGAACACTTCATAATTCCTGTTCTG	GGCTGTTTTGCAAAGAAAAATC	148
Jmjd2d	NM_173433	TTGACCGCTAGATTACTCCTCAC	TGTGAAAGCTGGGTGAGACAC	118
Jmjd3	NM_001017426	TACGTCCTGCACTTTCTTGGAC	CAGTTCCCACTTCTTCCCCTAC	103
Jmjd4	NM_178659	GGCCAGCAACTTAATTTACCTC	GGCATAGTGGCATGTGTGTATC	130
Jmjd5	NM_029842	TGGCTCTACTCCAGCTGTTCTC	GTTACATATGGGGCAAGTGGAC	107
Mina	NM_025910	TTGAGCATACATGACCCCTTTC	TCTGGCTCTTCTGTCATCTTCC	135
Phf2	NM_011078	TTATCCACTCCCACTTGACCTG	CAAGGACAGGGTCAAGGAAAAC	131
Phf8	NM_177201	TAAAAACAAACCCACCGCTTC	ACAAGGGGAACAAACAACAGAG	139
Pla2g4b	XM_355378	TTCTGGTGTGCCTGAAGATAGC	AACTCAGGACCTTTGGAAGAGC	133
Ptdsr (*Jmjd6*)	NM_033398	GACACCCAGAGAACAAGGACAC	GTTTCATTGGCACCATCCAC	111
Utx	NM_009483	AGCCTAGCTGGTCATTTCTTTG	AACAAGACAGAAATTCATAAAAGCAG	129
Uty	NM_009484	GGCATGGGAGGATAAATGATG	TCGTGCACAGTTCTGACAATG	134

Sequences are shown 5′ to 3′.

content of single cells. More than 40 EGFP-positive cells were analyzed in each experiment. The numbers of recovered EGFP-positive cells/dissected embryos were 43/5, 42/8, 61/3, 127/5, 58/2, 177/3, and 748/3 for E7.25, 7.75, 8.25, 8.75, 9.25, 9.75 and 10.5, respectively.

Single-cell cDNA analysis

Single-cell cDNAs from EB and EHF stage embryos were generated, and real-time quantitative PCR (Q-PCR) analyses were performed as described previously (Yabuta et al., 2006). The primer sequences used are listed in Table 1.

RESULTS

To investigate possible mechanisms involved in the epigenetic reprogramming in migrating PGCs (Seki et al., 2005), we explored the dynamics of this event using both *Blimp1*-mEGFP (Ohinata et al., 2005) and stella-EGFP transgenic mice (Payer et al., 2006), as well as anti-stella and anti-SSEA1 (Fox et al., 1981; Gomperts et al., 1994) antibody.

Blimp1-positive cells gradually acquire stella protein expression

To examine the manner of stella protein expression among the *Blimp1*-positive cells, we stained *Blimp1*-mEGFP embryos with anti-stella antibody. Consistent with the previous findings, we first detected that about 20% of the *Blimp1*-positive cells were weakly positive for stella at the LS stage (see Materials and methods for the staging of embryos) (see Fig. S1 in the supplementary material). At the EB stage, we detected stella in approximately 50% of *Blimp1*-positive cells. The number of stella-positive cells among *Blimp1*-positive cells increased progressively, and at the EHF stage as many as ~80% of *Blimp1*-positive cells showed stella expression (see Fig. S1 in the supplementary material) (Ohinata et al., 2005). The stella protein levels were, however, still very divergent, with *Blimp1*-positive cells migrating apart from the cluster generally bearing higher stella expression. All the stella-positive cells were *Blimp1*-positive. The numbers of stella-positive cells detected using antibodies and the stella-EGFP transgene were similar after the EHF stage. We therefore decided to use *Blimp1*-mEGFP embryos for detecting PGC precursors and PGCs mainly by the EHF stage and stella-EGFP embryos after the LHF stage.

Chromatin modifications in lineage-restricted precursors of PGCs

We first examined the global chromatin modification states of *Blimp1*-positive PGC precursors at the ES-LS stages by whole-mount immunohistochemistry using antibodies against specific modifications of histone N-terminal tails. We found that the staining patterns of these cells for the modifications H3K4me2, H3K4me3, H3K9Ac, H3K9me1, H3K9me2, H3K9me3, H3K27me2 and H3K27me3 (see Fig. S2 in the supplementary material and data not shown) were indistinguishable from those of their somatic mesodermal neighbors, some of which should share common precursors with the germ cell lineage. It is of note that the lineage-restricted PGC precursors in female embryos showed prominent accumulation of H3K27me3 in a single spot (see Fig. S2 in the supplementary material), most likely the inactive X chromosome (Erhardt et al., 2003; Plath et al., 2003; Silva et al., 2003), indicating that the initiation of the X-inactivation process in the germline is similar to that in the somatic lineages.

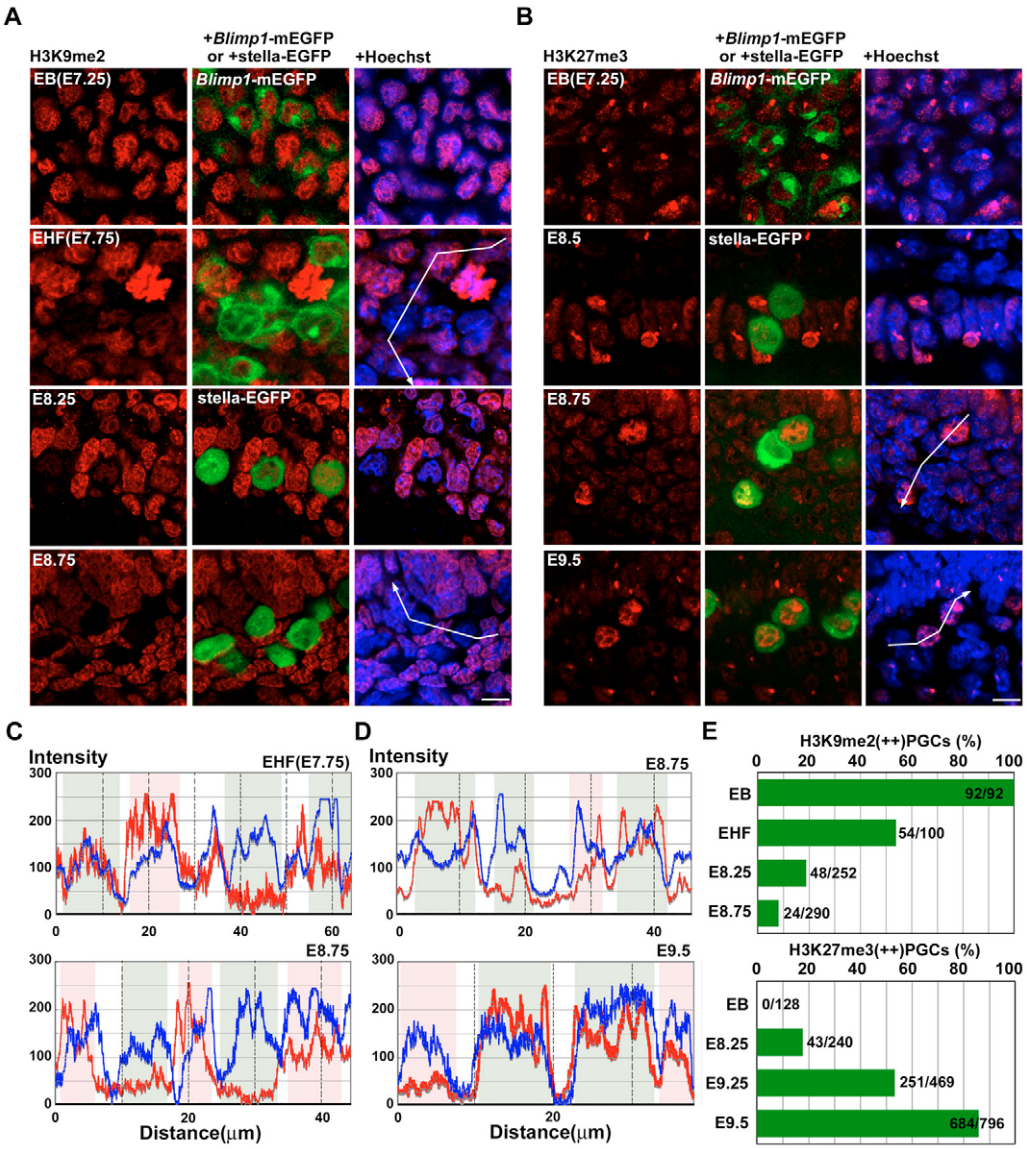

Fig. 1. Epigenetic reprogramming proceeds progressively in migrating PGCs in mice. (**A**) H3K9me2 (red, left column) in migrating PGCs (green, middle) at E7.25, E7.75, E8.25 and E8.75 as indicated. The white bent arrow indicates a line used for the line-scan plot in C. (**B**) H3K27me3 (red, left column) in migrating PGCs (green, middle) at E7.25, E8.5, E8.75 and E9.5 as indicated. Images merged with Hoechst staining (blue) are shown on the right (A,B). The white bent arrow indicates a line used for the line-scan plot analysis in D. (**C**) Line-scan plot of relative intensity of H3K9me2 (red) and Hoechst (blue). E7.75 (top) and E8.75 (bottom) cells shown in A. (**D**) Line-scan plot of relative intensity of H3K27me3 (red) and Hoechst (blue). E8.75 (top) and E9.5 (bottom) cells shown in B. The areas in C and D shaded in green and pink represent PGC and somatic cell nuclei, respectively. (**E**) Ratio of PGCs strongly positive for H3K9me2 (top) and for H3K27me3 (bottom) during the course of development. All PGCs from each embryo were analyzed. Scale bars: 10 μm in A,B.

Epigenetic reprogramming occurs progressively in migrating PGCs

We next set out to determine the precise onset and the completion of the erasure and upregulation of H3K9me2 and H3K27me3, respectively, in the developing PGC populations after the EB stage. As shown in Fig. 1A, PGCs showed similar levels of genome-wide H3K9me2 compared to their somatic neighbors at the EB stage. We first observed the PGCs with low H3K9me2 levels at the LB stage, and at the slightly later EHF stage nearly half of the PGCs appeared to show reduced H3K9me2 levels (Fig. 1A,C,E). Low H3K9me2 was more frequently seen in PGCs that initiated migration than in PGCs residing in a cluster (data not shown). At E8.25, more than 80% of the stella-positive PGCs showed low H3K9me2, and some of them had highly reduced levels of this modification. At E8.75, nearly all of the PGCs showed very low H3K9me2 levels (Fig. 1E). These findings indicate that H3K9me2 demethylation is initiated in some PGCs at around E7.5, that the ratio of H3K9me2 low PGCs increases along with development, and that the degree of demethylation in individual PGCs also increases along with development, reaching highly reduced levels at around E8.75. Regarding the upregulation of H3K27me3, we first identified stella-positive PGCs with higher levels of H3K27me3 at around E8.25. Both the percentage of PGCs with high levels of H3K27me3 and the degree of H3K27me3 upregulation in individual PGCs increased, as the development of PGCs proceeded (Fig. 2B,D,E), indicating that H3K27me3 upregulation in PGCs proceeds in a progressive, cell-by-cell manner, depending on their developmental maturation. We additionally found that PGCs at around E8.75 showed low levels of not only H3K9me2 but also H3K9me1 (see Fig. S3 in the supplementary material), indicating that the reprogramming event in PGCs effectively erases at least the mono- and di-methylated states of H3K9.

PGCs transiently repress RNA polymerase II-dependent transcription during epigenetic reprogramming

Because significant loss of repressive modifications might cause hyper-transcription, we next examined the global transcription state of PGCs using the antibody H5 (Patturajan et al., 1998). H5 recognizes phosphorylated Ser2 of the C-terminal domain (CTD) of RNA polymerase II (RNAP II), which is tightly associated with transcriptional elongation (Phatnani and

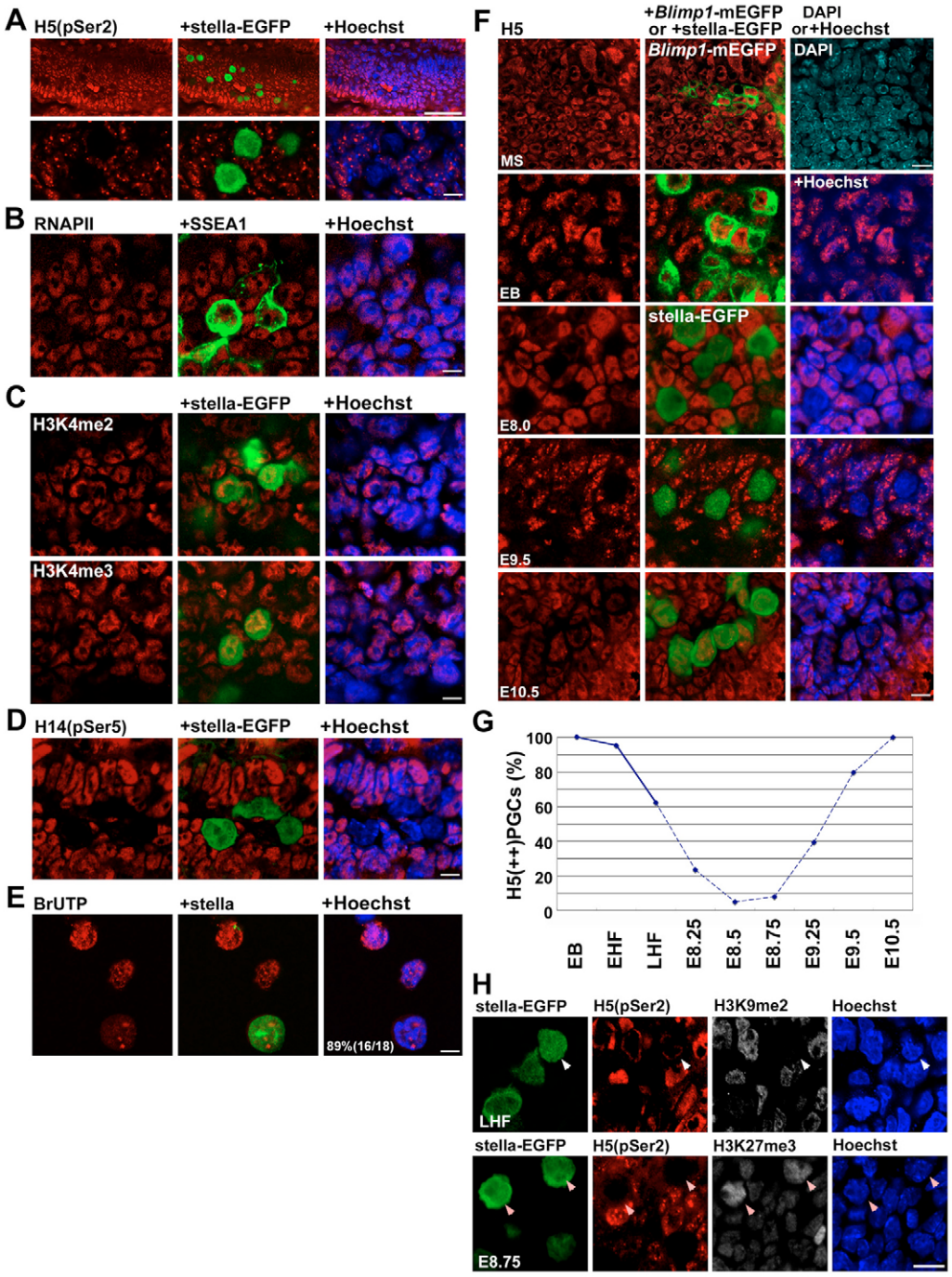

Fig. 2. Migrating PGCs exhibit transcriptional repression in mice. (**A**) (Top) Ser2 phosphorylation (red, left column) in PGCs (green, middle) at E8.75. (Bottom) Magnified images. (**B**) RNAP II expression (red, left) in PGCs (green, middle) at E8.75. (**C**) H3K4me2 (red, top, left) and H3K4me3 (red, bottom left) in migrating PGCs (green, middle) at E8.75. (**D**) Ser5 phosphorylation (red, left) in PGCs (green, middle) at E8.75. (**E**) BrUTP incorporation (red, left) in PGCs (green, middle) at E8.75. Percentages of BrUTP-weak, stella-positive cells are indicated with the number of cells analyzed in parenthesis (right). (**F**) Ser2 phosphorylation (red, left column) in PGCs (green, middle) at MS, E7.25, E8.0, E9.5 and E10.5 as indicated. An image for DAPI staining (F, MS) and images merged with Hoecsht staining (A-F, blue) are shown on the right. (**G**) Ratio of PGCs with strongly positive staining for Ser2 phosphorylation over the course of development. After E8.25 (dotted line), randomly chosen fragments were analyzed. (**H**) (Top) PGCs (green) stained by H5 (red), H3K9me2 (white) and Hoechst (blue) at E8.0. A white arrowhead denotes a PGC with reduced H3K9me2 but with Ser2 phosphorylation. (Bottom) PGCs (green) stained by H5 (red), H3K27me3 (white) and Hoechst (blue) at E8.75. Pink arrowheads denote PGCs with elevated H3K27me3 but without Ser2 phosphorylation. Scale bars: 100 μm in A, top row; 10 μm in A, bottom row; 10 μm in B-H.

Greenleaf, 2006) and is a good marker for the global transcriptional activity of a wide range of cell types. We first examined CTD Ser2 phosphorylation in PGCs at E8.75. Contrary to our expectation, PGCs at this stage showed extremely low levels of this modification (Fig. 2A). This was not due to the PGC-specific downregulation of RNAP II itself, as the levels of RNAP II protein detected in PGCs were comparable to those detected in their somatic neighbors by the same immunohistochemical method (Fig. 2B). We then examined the global distribution and the levels of H3K4me2 and H3K4me3 that were associated with transcriptionally permissive/active states and found that the distribution and levels of these modifications in PGCs were similar to those in their somatic neighbors (Fig. 2C), suggesting that PGCs at E8.75 repress RNAP II-dependent transcription by a mechanism independent of their chromatin modification states.

To determine the step at which PGCs may abort RNAP II-dependent transcription, we next stained PGCs at E8.75 with the antibody H14 that recognizes phosphorylated Ser5 of RNAP II CTD, which is associated with the transition from transcriptional initiation to promoter clearance (Phatnani and Greenleaf, 2006). We found that, in contrast to their somatic neighbors, PGCs were again essentially negative for Ser5 phosphorylation (Fig. 2D), indicating that the global transcription in migrating PGCs is halted at a step before the transition from the initiation complex formation to promoter clearance.

To further monitor the transcription state of PGCs, we performed BrUTP incorporation experiments to examine nascent RNA synthesis at E8.75. As shown in Fig. 2E, somatic cells negative for stella showed strong BrUTP incorporation in their nucleoplasm, whereas approximately 90% of stella-positive PGCs exhibited weak nucleoplasmic BrUTP incorporation, except for a few intensive foci that were negative for DAPI and most likely nucleoli, indicating that migrating PGCs at E8.75 specifically repress RNAP II-dependent transcription with the RNAP I-dependent ribosomal RNA transcription kept constant.

We next examined the onset and the duration of the loss of CTD Ser2 phosphorylation in PGCs (Fig. 2F). *Blimp1*-positive PGC precursors at the ES-LS stages showed indistinguishable staining of CTD phosphorylation compared to their somatic neighbors and epiblast cells, indicating that these cells undergo active transcription, consistent with the finding that PGC precursors showed decent levels of H3K4me2, me3 and H3K9ac (see Fig. S2 in the supplementary material). Up until the EHF stage, most PGCs showed CTD phosphorylation. However, at the LHF stage (E8.0), many PGCs lost this modification (Fig. 2F,G). The percentage of PGCs negative for CTD phosphorylation increased gradually during development, and at E8.5-8.75, most PGCs detected by stella-EGFP lacked this modification (Fig. 2F,G), as we initially observed. At E9.25, some PGCs regained this modification, and by E10.5, staining for CTD phosphorylation was apparent in almost all the PGCs (Fig. 2F,G). These findings indicate that PGCs turned off RNAP II-dependent transcription transiently and in a cell-by-cell manner during their migration period, and this was presumably achieved through a mechanism independent from chromatin-based silencing.

Relationship between chromatin remodeling and transcriptional quiescence

Our timecourse analyses demonstrated that the reduction of H3K9me2 was first observed as early as E7.75 (EHF stage) in 54% of PGCs, whereas loss of transcriptional activity was still not evident in most PGCs at the same stage. By contrast, the upregulation of H3K27me3 commenced as early as E8.25, when PGCs were progressively losing RNAP II CTD phosphorylation, which was recovered in some PGCs only at E9.0~9.25. These findings indicate that a cascade of events takes place in individual PGCs, with the reduction of H3K9me2 occurring first, and the loss of RNAP II CTD phosphorylation second, followed by upregulation of H3K27me27 and subsequent resumption of RNAP II-dependent transcription. To confirm this, we performed whole-mount triple labeling, which demonstrated that some PGCs in which the reduction of H3K9me2 had already started at E8.0 had not yet established the transcriptional quiescence (Fig. 2H, white arrowhead). We also found that the upregulation of genome-wide H3K27me3 preceded the restoration of RNAP II-dependent transcriptional activity in PGCs at E8.75 (Fig. 2H, pink arrowhead), consistent with the proposed sequence of events in PGCs. The emergence of PGCs with hyper-H3K27me3 from H5-negative PGCs indicated that de novo transcription driven by RNA polymerase II was not required for hyper-H3K27me3 in PGCs.

Epigenetic reprogramming proceeds in the prolonged G2 phase of the cell cycle

We next explored the cell cycle state of the migrating PGCs when all the observed events were apparently occurring in an ordered manner. To this end, we first examined the increase of PGC number using *Blimp1*-mEGFP (from LS to EHF stage) and stella-EGFP embryos as well as anti-stella antibody staining (from E8.0 onwards). As shown in Fig. 3A (see also Table S1 in the supplementary material), although the number of PGCs varied considerably even among embryos at similar developmental stages, the increase of overall PGC number between E8.0 and E9.0~9.25, coincident with the epigenetic reprogramming, seemed slower than that after E9.5.

We therefore performed BrdU labeling to assess the S-phase entry of PGCs at each stage of development. We injected the pregnant females with BrdU intraperitoneally and isolated their embryos 6 hours later to evaluate the incorporation of BrdU into embryonic cells. We found that *Blimp1*-positive PGC precursors and PGCs in isolated embryos at the LS stage showed approximately 50% BrdU incorporation (Fig. 3A,B), indicating that 50% of *Blimp1*-positive cells had entered into S-phase in the previous 6 hours. Subsequently, however, the percentage of the BrdU-positive *Blimp1*-positive cells decreased to as low as 15% at the EHF stage, and the percentage of BrdU-positive, stella-positive PGCs remained low until around E9.0 (Fig. 3A,B). By contrast, more than half of the surrounding somatic cells incorporated BrdU throughout the stages examined. Consistent with our counting of PGC number, stella-positive PGCs that incorporated BrdU increased after E9.25 and reached approximately 50% at E9.75, which remained constant until at least E10.5 (Fig. 3A,B). These results indicate that a majority of PGCs from about E7.5 up until E9.0 did not enter into S-phase and may be blocked at a certain stage of the cell cycle.

To explore the cell cycle phase of the migrating PGCs, we analyzed the expression of cyclin B1, which accumulates at high levels in the cytoplasm at the late G2 phase of the cell cycle (Pines and Hunter, 1991). At the LB to EHF stage, about 20% of the *Blimp1*-positive PGCs showed a high concentration of cyclin B1 in their cytoplasm (Fig. 3A,C). Subsequently, after E8.0 onwards, the percentage of PGCs that were strongly positive for cyclin B1 increased progressively, and it reached as high as 80% at E8.5 to 8.75. The high percentage of PGCs showing strong positivity for cyclin B1 persisted up until E9.5 and sharply decreased after E9.75 (Fig. 3A,C). Collectively, these findings suggest that a majority of migrating PGCs are blocked at the G2 phase of the cell cycle.

Finally, we examined the DNA content of PGCs by FACS analysis. As shown in Fig. 3D, embryonic cells negative for *Blimp1*-mEGFP or stella-EGFP showed a clear G1 peak with a broad S-phase and a less prominent G2 peak. This cell cycle distribution of embryonic somatic cells resembles that of embryonic stem cells (Fujii-Yamamoto et al., 2005) and indicates a rapidly cycling cell population. We found that *Blimp1*-positive cells at E7.25 showed a similar cell cycle distribution. By contrast, however, a majority of stella-positive cells from E7.75 to 8.75 (approximately 60%) were found to be at the G2 phase, consistent with the BrdU incorporation and cyclin B1 immunostaining analyses. At E10.5, stella-negative cells showed a typical somatic cell cycle distribution with a very prominent G1 peak, whereas stella-positive PGCs were distributed almost equally in the G1 (29.7%), S (34.4%) and G2 (35.4%) phases, indicating that PGCs at this stage are rapidly cycling. Collectively, our findings indicate that a majority of PGCs enter the G2 arrest of the cell cycle at some point between E7.75 and 8.75, which is when H3K9me2 demethylation, transcriptional quiescence and H3K27me3 upregulation proceed.

Nanos3 is not involved in the epigenetic reprogramming and transcriptional quiescence

To gain insight into the molecular mechanisms underlying the epigenetic reprogramming, we first analyzed the genome-wide epigenetic properties of *Nanos3*-deficient PGCs. Nanos is an

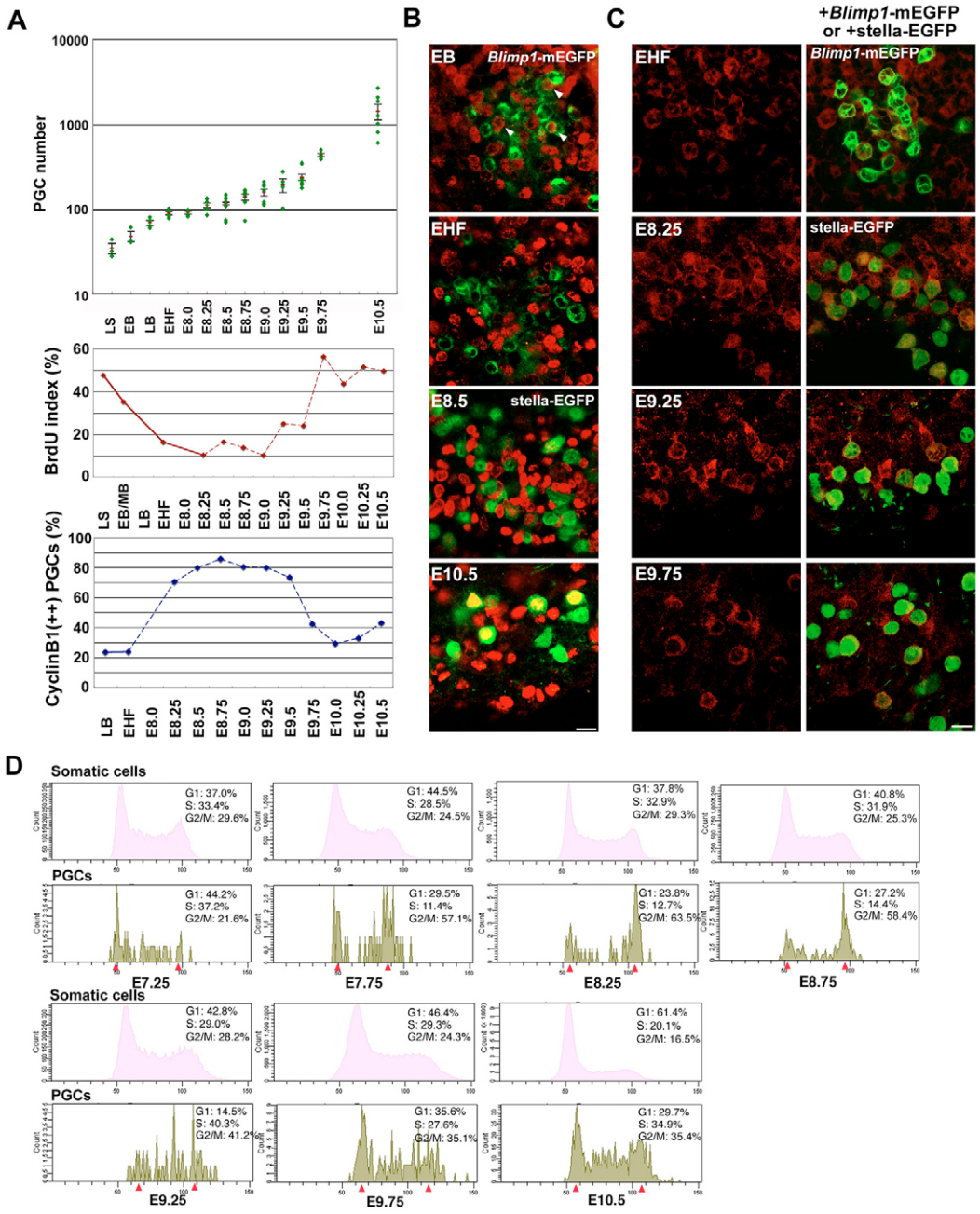

Fig. 3. Cell cycle distribution of migrating PGCs. (**A**) PGC number with average and standard deviation (top), ratio of PGCs with BrdU (middle) and with cyclin B1-strong-positivity (bottom) over the course of development in mice. After E8.25 (dotted line), randomly chosen cells were analyzed for BrdU incorporation and cyclin B1 immunostaining. (**B**) Representative images of BrdU incorporation (red) into PGCs (green) at E7.25, E7.75, E8.5 and E10.5 as indicated. (**C**) Representative images of cyclin B1 immunoreactivity (red, left column) in PGCs (green, right) at E7.75, E8.25, E9.25 and E9.75 as indicated. (**D**) FACS analysis of the cell cycle distribution of PGCs (green) and embryonic somatic cells (pink) during the course of development. Red arrowheads denote the G1 and G2 peaks. Scale bars: 10 μm in B,C.

evolutionally conserved protein essential for germ cell development (Kobayashi et al., 1996; Subramaniam and Seydoux, 1999; Wang and Lehmann, 1991; Tsuda et al., 2003) and is required to maintain low H3K4 methylation levels (*C. elegans* and *D. melanogaster*) and to prevent premature zygotic transcription (*D. melanogaster*) in PGCs (Schaner et al., 2003). In the mouse, *Nanos3* is expressed in PGCs after E7.25 (Yabuta et al., 2006) and is indispensable for their subsequent development (Tsuda et al., 2003), making it a good candidate for involvement in the epigenetic reprogramming in migrating PGCs. However, *Nanos3* mutant PGCs appeared to show the proper H3K9me2 demethylation at E8.75 and H3K27me3 upregulation at E9.5 (Fig. 4A,B). The level of H3K4me2 in *Nanos3* mutant cells also looked indistinguishable from that of wild-type PGCs (Fig. 4C). Moreover, quiescence of RNAP II-dependent transcription seemed to occur normally in the absence of Nanos3 (Fig. 4D). These findings indicate that the genome-wide epigenetic reprogramming and transcriptional quiescence in mouse PGCs are independent from Nanos function.

Expression of the JmjC domain-containing histone demethylase family

Recent studies have been identifying enzymes responsible for direct histone demethylation that contain JumonjiC (JmjC) domains (Klose et al., 2006). Therefore, we examined the expression of all the members of the JmjC domain-containing genes in the mouse genome by Q-PCR using single-cell cDNAs prepared from PGCs and their somatic neighbors at the EB and the EHF stages (Yabuta et al., 2006). Although this analysis identified that many members of this family of proteins including *Jmjd1a* (*Jhdm2a*), a demethylase for H3K9me1 and me2, were

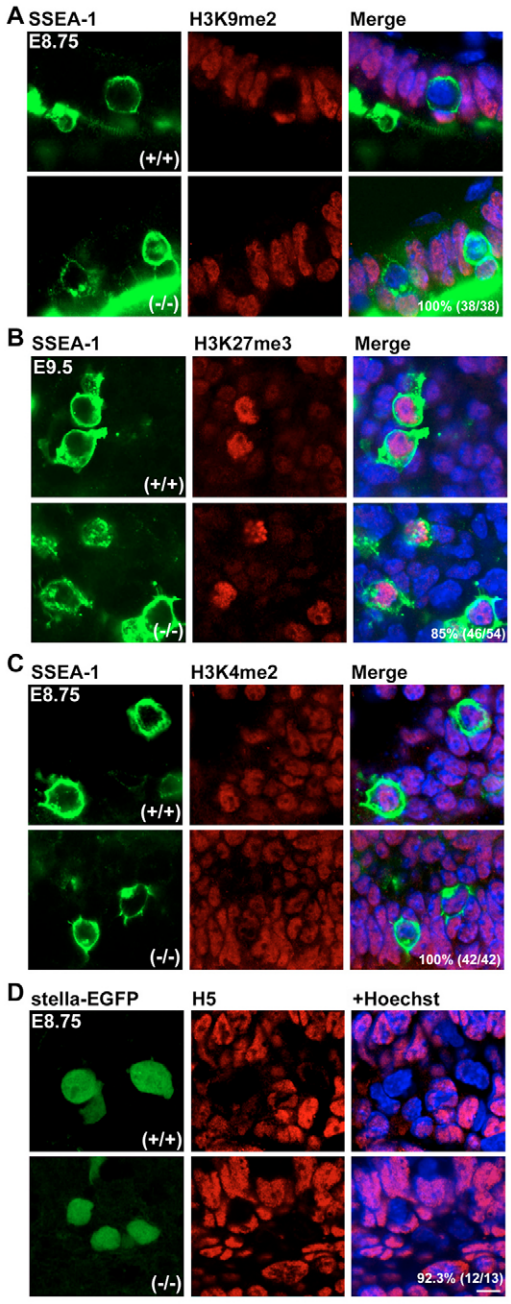

Fig. 4. Epigenetic reprogramming and transcriptional quiescence are independent of Nanos3 function in mice. H3K9me2 (**A**), H3K27me3 (**B**), H3K4me2 (**C**) and Ser2 phosphorylation (**D**) (red, middle columns) in wild-type (+/+) (top row) and *Nanos3*-null (–/–) (bottom row) PGCs (green, left columns). Merged images with Hoechst staining (blue) are shown in the right columns. Percentages of H3K9me2-reduced (A), H3K27me3-elevated (B), H3K4me2-normal (C) and H5-negative (D) PGCs are indicated with the number of cells analyzed in parenthesis. Scale bar: 10 μm.

indeed expressed in PGCs at these stages, none of them were specific to PGCs as seen for genes such as *Blimp1* and stella (Fig. 5; see Fig. S4 in the supplementary material), suggesting that PGCs may possess an additional mechanism to direct genome-wide demethylation of H3K9.

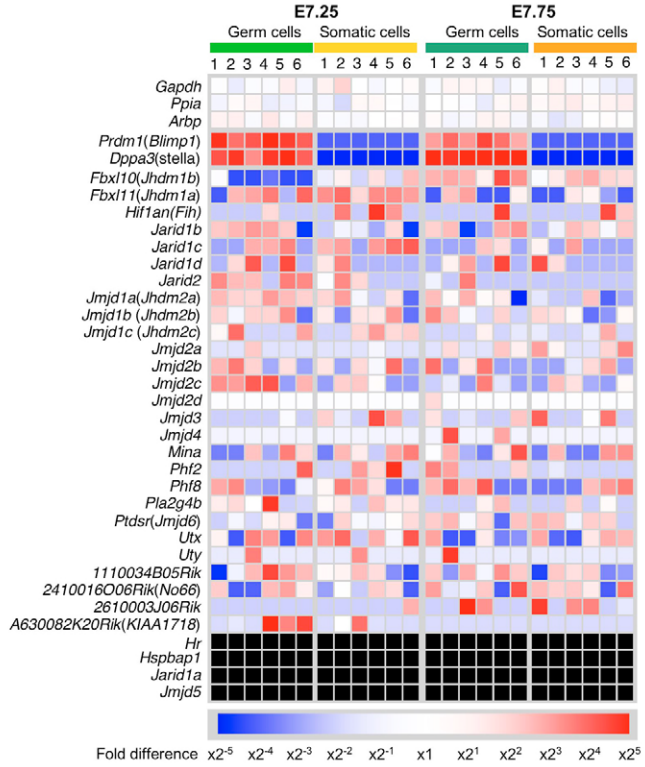

Fig. 5. Heatmap representation of the expression of JmjC domain-containing genes in murine PGCs and their somatic neighbors. The expression levels relative to the average in all 24 cells are represented by a color code shown at the bottom, with corresponding fold difference values. Genes, the expression of which was not detected in all 24 cells, are shown in black.

Specific downregulation of a key histone methyltransferase before H3K9me2 demethylation

As a candidate for this putative mechanism, we previously found that *Glp* (also known as *Ehmt1*), a gene encoding a histone methyltransferase essential for conferring H3K9me2 in early embryos (Tachibana et al., 2005), was downregulated as early as E7.25 specifically in PGCs (Yabuta et al., 2006) and was the only gene among the SET-domain-containing genes in the mouse genome that showed enrichment in somatic neighbors (data not shown). GLP was shown to form a complex with G9a and to be essential for the stability and the histone methyltransferase activity of this complex. Thus, lack of either GLP or G9a alone is considered to lead to the loss of function of this enzyme complex, leading us to speculate that downregulation of *Glp* might be crucial for the genome-wide demethylation of H3K9me2 in PGCs. To address this point, we examined the expression of GLP and G9a proteins in embryos by whole-mount immunofluorescence analysis. Consistent with our previous single-cell Q-PCR analysis, at the EHF stage, *Blimp1*-positive cells, especially those migrating toward the endoderm, already repressed GLP expression (Fig. 6A). By contrast, somatic neighbors expressed GLP almost uniformly at this stage. It is of note that some of the *Blimp1*-positive cells forming a cluster at the base of the allantois showed GLP

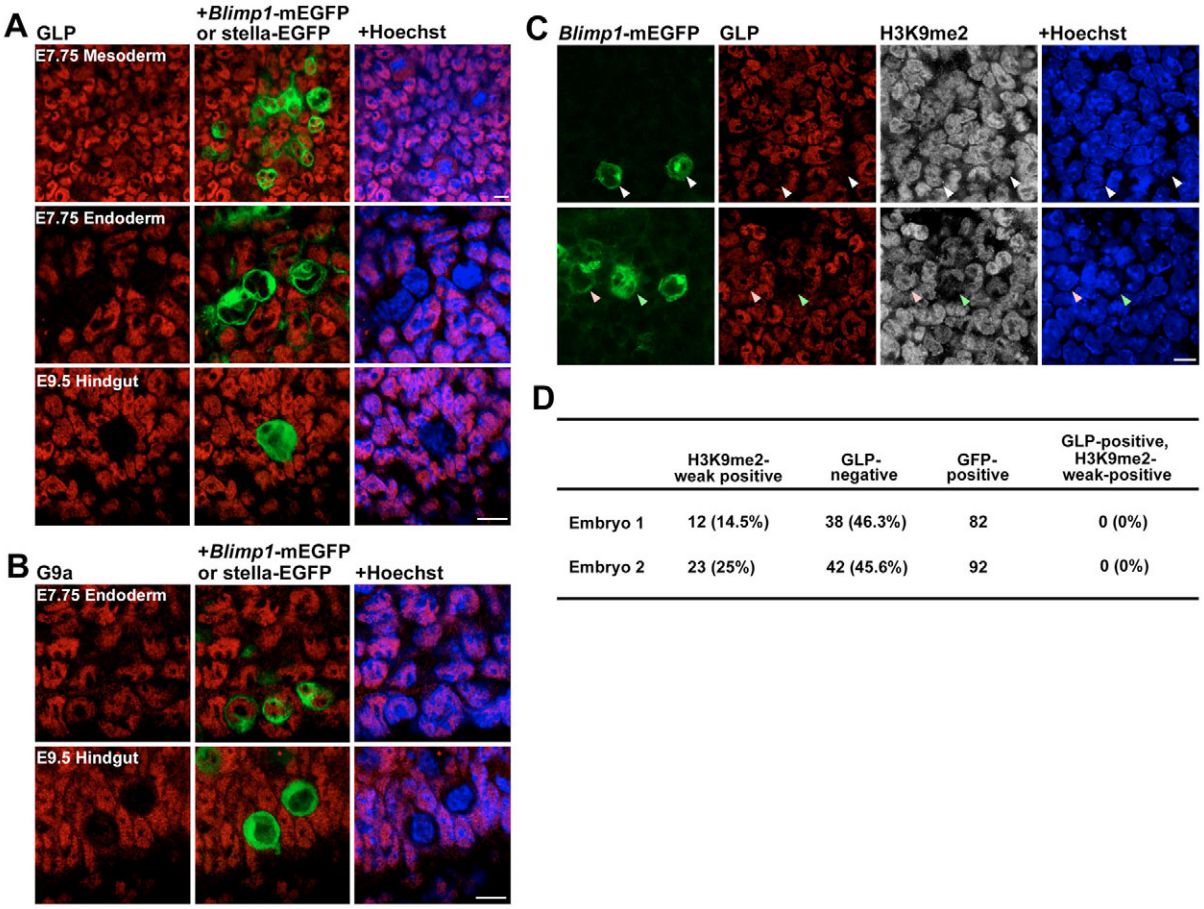

D

	H3K9me2-weak positive	GLP-negative	GFP-positive	GLP-positive, H3K9me2-weak-positive
Embryo 1	12 (14.5%)	38 (46.3%)	82	0 (0%)
Embryo 2	23 (25%)	42 (45.6%)	92	0 (0%)

Fig. 6. Specific repression of GLP in murine PGCs before their epigenetic reprogramming. (**A**) GLP expression (red, left) in PGCs (green, middle) in the extra-embryonic mesoderm at E7.75, and in the developing hindgut endoderm at E7.75 and E9.5 as indicated. (**B**) G9a expression (red, left) in PGCs (green, middle) in the developing hindgut endoderm at E7.75 (top) and at E9.5 (bottom). Images merged with Hoechst staining (blue) are shown on the right (A,B). (**C**) Triple staining of *Blimp1*-positive cells (green), GLP (red) and H3K9me2 (white), in addition to Hoechst (blue) at E7.5 (LB). Two representative fields are shown. Arrowheads indicate PGCs with repressed GLP but with high H3K9me2 (white), with high GLP with high H3K9me2 (pink), and with repressed GLP and reduced H3K9me2 (green). (**D**) Number and percentage (in parenthesis) of H3K9me2 weak-, GLP-negative and GLP-positive and H3K9me2 weak-cells among *Blimp1*-positive cells in two LB-stage embryos. Scale bars: 10 μm in A-C.

expression (Fig. 6A), suggesting that GLP is repressed progressively in migrating PGCs. Thereafter, we could not detect GLP expression in PGCs until at least E10.5. By contrast, G9a was detected at E7.75 but was significantly reduced in PGCs at E9.5 (Fig. 6B). These findings indicate that PGCs downregulate GLP at around E7.5~7.75 and G9a at around E9.0, resulting in the loss of two essential enzymes for genome-wide H3K9me2.

We next explored whether the downregulation of GLP occurs before global demethylation of H3K9me2 in PGCs. For this purpose, we examined the correlation between downregulation of GLP and demethylation of H3K9me2 at the LB stage (E7.5), at which some PGCs begin to show reduced H3K9me2. At this stage, about 15-25% of *Blimp1*-positive cells already showed reduced H3K9me2 levels and all of them showed GLP repression (Fig. 6C,D). However, approximately 45% of *Blimp1*-positive cells showed GLP repression, but more than 50% of them still showed high levels of H3K9me2 (Fig. 6D). No PGCs with GLP were negative for H3K9me2. These findings demonstrate that downregulation of GLP occurs before the global demethylation of H3K9me2 in PGCs.

DISCUSSION

An ordered sequence of events during the migration of PGCs

We have provided a first in-depth analysis of the cellular dynamics of migrating PGCs in mice that are undergoing genome-wide epigenetic reprogramming (see Fig. 7 for summary). Contrary to previous assumptions (Lawson and Hage, 1994; Tam and Snow, 1981), we found that the number of PGCs does not increase at a constant rate. This finding was possible due to the high sensitivity of the PGC reporter mice used in this study, which enabled more accurate counting of PGC numbers in the early stages (~E8.25) than the classical AP staining, which has been shown to frequently underestimate the PGC number in the early stages (Lawson et al., 1999). The increase of PGC number from around E8.0 to 9.0, when most PGCs are migrating in the hindgut endoderm, was relatively slower, and a majority (~60%) of stella-positive PGCs were in the G2 phase of the cell cycle. Epigenetic reprogramming proceeds progressively in this period in individual PGCs. It would therefore be likely that the progressive removal of H3K9me2, transcriptional repression and H3K27me3 upregulation all occur in the G2 phase of one particular cell cycle. As the decrease of H3K9me2

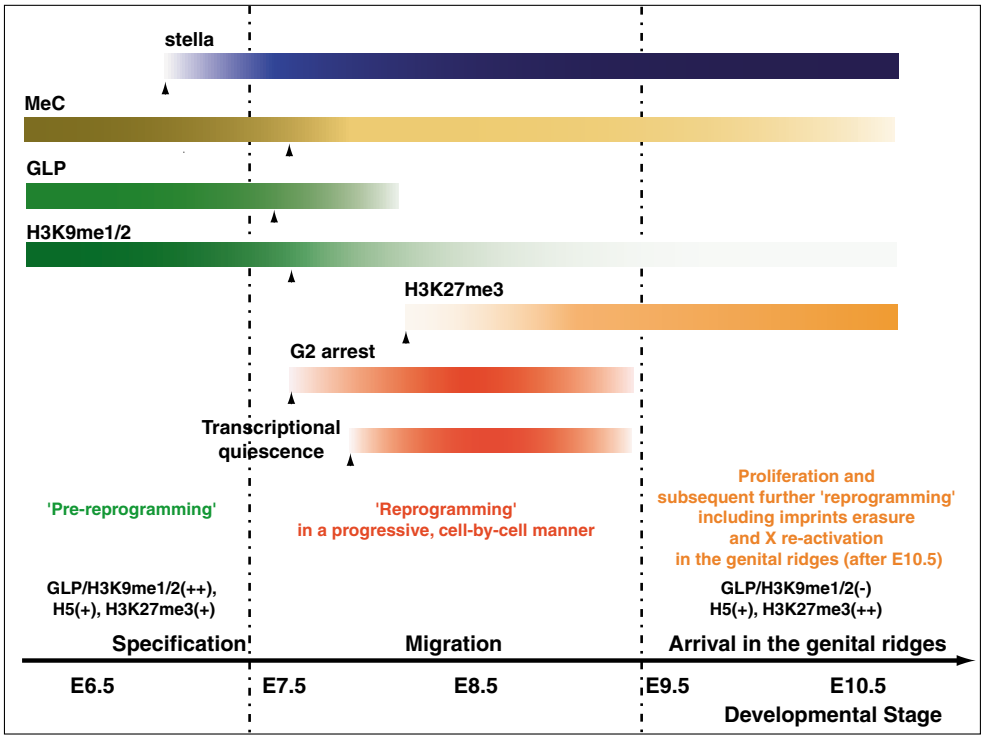

Fig. 7. Cellular dynamics and epigenetic reprogramming in migrating PGCs in mice. Events identified in both the current and previous (Seki et al., 2005) studies are shown.

immunoreactivity seemed greater than twofold (Fig. 1C), this process would not be explained by a simple passive dilution associated with the doubling of chromosomes.

What, then, is the molecular basis of this phenomenon? We found that some of the recently identified histone demethylases with JmjC domains (Klose et al., 2006) were indeed expressed in PGCs, but their expressions were similarly seen in somatic neighbors, suggesting that PGCs might have additional mechanisms allowing genome-wide removal of H3K9me2. As one such mechanism, we identified that PGCs specifically repress an essential H3K9 methyltransferase, GLP, at around the LB stage just before the reduction of H3K9me2 in some PGCs, suggesting that repression of an active enzyme triggers genome-wide loss of H3K9me2, either through a turnover of methyl groups or a replacement of the entire H3 with unmodified H3. Consistently, a mass spectrometry analysis of H3K9 methyl groups differentially pulse-labeled by a heavy isotope demonstrated that H3K9me2 turns over without replication (Fodor et al., 2006). Furthermore, it was recently reported that chromatin-associated histones and non-chromatin-associated histones are continually exchanged in *Xenopus* oocytes, and maintenance of H3K9 methylation at a specific site requires the continual presence of an H3K9 histone methyltransferase (Stewart et al., 2006). Thus, repression of an essential enzyme may shift the equilibrium between methylation and demethylation toward demethylation, leading to the erasure of H3K9me2, possibly through these mechanisms, in migrating PGCs. This is consistent with our additional finding that PGCs also showed low H3K9me1, another modification mediated by G9a-GLP complex (Tachibana et al., 2005).

Another finding of note is that, after the onset of H3K9me2 demethylation, PGCs appeared to paradoxically repress RNAP II-dependent transcription. Although the functional significance of this phenomenon is currently unknown, it may be crucial to protect the cells from deregulated transcription in the absence of major chromatin-based repressive mechanisms during epigenetic reprogramming. Consistently, this transcriptional repression ensues until PGCs acquire high levels of H3K27me3 and is relieved gradually afterwards, which seems concomitant with their release from the G2 arrest and rapid proliferation. Further studies will be needed to clarify the significance of this event as well as to identify the mechanism by which H3K27me3 is specifically upregulated.

A comparison with the cellular dynamics of PGCs in other organisms

This study makes it possible to compare the cellular dynamics of PGCs in mice with those of other organisms that specify the germ cell lineage with the 'preformation' mode. In *C. elegans*, the germline precursor blastomeres P1 to P4 repress RNAP II-dependent transcription (Seydoux and Dunn, 1997). Although they exhibit genome-wide H3K4 methylation at a similar level to their somatic neighbors, they specifically express PIE-1, which prevents phosphorylation of RNAP II CTD by competing with the CDK-9–cyclin T complex (Zhang et al., 2003). P4 blastomeres divide to form Z2 and Z3 cells, the lineage-restricted PGCs, which then degrade PIE-1 and become positive for the phosphorylation of RNAP II CTD (Schaner et al., 2003). However, these cells lose their genome-wide H3K4 methylation and appear to transcribe only a few genes and to become mitotically quiescent until the embryo hatches (Schaner and Kelly, 2006).

In *Drosophila*, pole cells, the lineage-restricted PGCs also exhibit transcriptional quiescence with no RNAP II CTD phosphorylation, low H3K4 methylation and high H3K9 methylation levels (Schaner et al., 2003; Seydoux and Dunn, 1997). This transcriptional repression depends on *pgc* (Deshpande et al., 2004; Martinho et al., 2004; Nakamura et al., 1996). After asynchronous zero to two divisions, they become mitotically quiescent at the G2 phase (Su et al., 1998) and undergo migration. It therefore seems to be the case that PGC precursors and PGCs in *C. elegans* and PGCs in

Drosophila show no or very low levels of transcription with initial chromatin-independent and subsequent chromatin-dependent mechanisms. Interestingly, in both *C. elegans* and *Drosophila*, Nanos activity is required to maintain the low H3K4 methylation levels in PGCs (Schaner et al., 2003).

By contrast, in mice, we showed that *Blimp1*-positive PGC precursors and stella-positive PGCs are transcriptionally active with phosphorylated RNAP II CTD by E7.75, consistent with the activation of many specific genes associated with germ cell specification (Yabuta et al., 2006). Nonetheless, we found that migrating PGCs transiently exhibit repression of RNAP II-dependent transcription, an event that appears to be similar to those observed in *C. elegans* and *Drosophila*. However, this seems to be associated with epigenetic reprogramming and is not likely to be a mechanism to prevent somatic gene expression in PGCs. Furthermore, we showed that neither chromatin modifications nor transcriptional quiescence were affected in the absence of Nanos3, suggesting that this protein is not involved in these events in mice. Our observation that most migrating PGCs in mice are in the G2 phase of the cell cycle may suggest a similarity to the situation in *Drosophila* pole cells. Although the functional significance of the G2 arrest in migrating pole cells is unclear, the G2 arrest of migrating PGCs in mice again seems tightly associated with the epigenetic reprogramming. Therefore, repression of RNAP II-dependent transcription and G2 arrest of the cell cycle in mice may be independently acquired events for the epigenetic reprogramming to occur efficiently, although these events are commonly observed in three distinct organisms.

Perspective

This study clarified, for the first time, a sequence of unique events occurring in migrating PGCs in mice that undergo genome-wide epigenetic reprogramming, which may have general implications for somatic cell reprogrammings of any kind. Recently, it was shown that PGCs elevate H4R2 and H2AR3 methylation at around E8.5 through an action of the Blimp1-Prmt5 complex (Ancelin et al., 2006), demonstrating that PGCs undergo yet another level of complex epigenetic programming in their migration. These events precede reactivation of the inactive X chromosome in female PGCs and erasure of parental imprints, both of which occur when PGCs colonise the genital ridges (Li, 2002; McLaren, 2003; Surani, 2001). The precise relevance of the earlier events reported in this study to those in the genital ridges is, however, currently unknown. A crucial step to resolve this issue would be to determine the target sequences from which H3K9me2 is removed and upon which H3K27me3 is imposed in migrating PGCs. There is currently only a limited amount of information available regarding the genome-wide distribution of these two modifications in mammalian cells in general (Bernstein et al., 2007). We consider it an essential challenge to develop an experimental system that allows genome-wide analysis of specific histone modifications from a small amount of biological samples, as in the case for PGCs.

We are grateful to M. Azim Surani for the stella-EGFP BAC plasmid, Etsuko Hasegawa for her help on FACS analysis, and Mike Royle for his help in preparing this manuscript. Y.S. is a fellow of the Special Postdoctoral Researchers Program of RIKEN. This study was supported in part by a Grant-in-Aid from the Ministry of Education, Culture, Sports, Science, and Technology of Japan, and by a PRESTO project grant from the Japan Science and Technology Agency.

Supplementary material

Supplementary material for this article is available at http://dev.biologists.org/cgi/content/full/134/14/2627/DC1

References

Ancelin, K., Lange, U. C., Hajkova, P., Schneider, R., Bannister, A. J., Kouzarides, T. and Surani, M. A. (2006). Blimp1 associates with Prmt5 and directs histone arginine methylation in mouse germ cells. *Nat. Cell Biol.* **8**, 623-630.

Bernstein, B. E., Meissner, A. and Lander, E. S. (2007). The mammalian epigenome. *Cell* **128**, 669-681.

Bird, A. (2002). DNA methylation patterns and epigenetic memory. *Genes Dev.* **16**, 6-21.

Deshpande, G., Calhoun, G. and Schedl, P. (2004). Overlapping mechanisms function to establish transcriptional quiescence in the embryonic Drosophila germline. *Development* **131**, 1247-1257.

Downs, K. M. and Davies, T. (1993). Staging of gastrulating mouse embryos by morphological landmarks in the dissecting microscope. *Development* **118**, 1255-1266.

Erhardt, S., Su, I. H., Schneider, R., Barton, S., Bannister, A. J., Perez-Burgos, L., Jenuwein, T., Kouzarides, T., Tarakhovsky, A. and Surani, M. A. (2003). Consequences of the depletion of zygotic and embryonic enhancer of zeste 2 during preimplantation mouse development. *Development* **130**, 4235-4248.

Extavour, C. G. and Akam, M. (2003). Mechanisms of germ cell specification across the metazoans: epigenesis and preformation. *Development* **130**, 5869-5884.

Fodor, B. D., Kubicek, S., Yonezawa, M., O'Sullivan, R. J., Sengupta, R., Perez-Burgos, L., Opravil, S., Mechtler, K., Schotta, G. and Jenuwein, T. (2006). Jmjd2b antagonizes H3K9 trimethylation at pericentric heterochromatin in mammalian cells. *Genes Dev.* **20**, 1557-1562.

Fox, N., Damjanov, I., Martinez-Hernandez, A., Knowles, B. B. and Solter, D. (1981). Immunohistochemical localization of the early embryonic antigen (SSEA-1) in postimplantation mouse embryos and fetal and adult tissues. *Dev. Biol.* **83**, 391-398.

Fujii-Yamamoto, H., Kim, J. M., Arai, K. and Masai, H. (2005). Cell cycle and developmental regulations of replication factors in mouse embryonic stem cells. *J. Biol. Chem.* **280**, 12976-12987.

Gomperts, M., Garcia-Castro, M., Wylie, C. and Heasman, J. (1994). Interactions between primordial germ cells play a role in their migration in mouse embryos. *Development* **120**, 135-141.

Klose, R. J., Kallin, E. M. and Zhang, Y. (2006). JmjC-domain-containing proteins and histone demethylation. *Nat. Rev. Genet.* **7**, 715-727.

Kobayashi, S., Yamada, M., Asaoka, M. and Kitamura, T. (1996). Essential role of the posterior morphogen nanos for germline development in Drosophila. *Nature* **380**, 708-711.

Lawson, K. A. and Hage, W. J. (1994). Clonal analysis of the origin of primordial germ cells in the mouse. *Ciba Found. Symp.* **182**, 68-84.

Lawson, K. A., Dunn, N. R., Roelen, B. A., Zeinstra, L. M., Davis, A. M., Wright, C. V., Korving, J. P. and Hogan, B. L. (1999). Bmp4 is required for the generation of primordial germ cells in the mouse embryo. *Genes Dev.* **13**, 424-436.

Li, E. (2002). Chromatin modification and epigenetic reprogramming in mammalian development. *Nat. Rev. Genet.* **3**, 662-673.

Martin, C. and Zhang, Y. (2005). The diverse functions of histone lysine methylation. *Nat. Rev. Mol. Cell Biol.* **6**, 838-849.

Martinho, R. G., Kunwar, P. S., Casanova, J. and Lehmann, R. (2004). A noncoding RNA is required for the repression of RNApolII-dependent transcription in primordial germ cells. *Curr. Biol.* **14**, 159-165.

McLaren, A. (2003). Primordial germ cells in the mouse. *Dev. Biol.* **262**, 1-15.

Nakamura, A., Amikura, R., Mukai, M., Kobayashi, S. and Lasko, P. F. (1996). Requirement for a noncoding RNA in Drosophila polar granules for germ cell establishment. *Science* **274**, 2075-2079.

Ohinata, Y., Payer, B., O'Carroll, D., Ancelin, K., Ono, Y., Sano, M., Barton, S. C., Obukhanych, T., Nussenzweig, M., Tarakhovsky, A. et al. (2005). Blimp1 is a critical determinant of the germ cell lineage in mice. *Nature* **436**, 207-213.

Ohinata, Y., Seki, Y., Payer, B., O'Carroll, D., Surani, M. A. and Saitou, M. (2006). Germline recruitment in mice: a genetic program for epigenetic reprogramming. *Ernst Schering Res. Found. Workshop* **2006**, 143-174.

Patturajan, M., Schulte, R. J., Sefton, B. M., Berezney, R., Vincent, M., Bensaude, O., Warren, S. L. and Corden, J. L. (1998). Growth-related changes in phosphorylation of yeast RNA polymerase II. *J. Biol. Chem.* **273**, 4689-4694.

Payer, B., Chuva de Sousa Lopes, S. M., Barton, S. C., Lee, C., Saitou, M. and Surani, M. A. (2006). Generation of stella-GFP transgenic mice: a novel tool to study germ cell development. *Genesis* **44**, 75-83.

Peters, A. H. and Schubeler, D. (2005). Methylation of histones: playing memory with DNA. *Curr. Opin. Cell Biol.* **17**, 230-238.

Phatnani, H. P. and Greenleaf, A. L. (2006). Phosphorylation and functions of the RNA polymerase II CTD. *Genes Dev.* **20**, 2922-2936.

Pines, J. and Hunter, T. (1991). Human cyclins A and B1 are differentially located in the cell and undergo cell cycle-dependent nuclear transport. *J. Cell Biol.* **115**, 1-17.

Plath, K., Fang, J., Mlynarczyk-Evans, S. K., Cao, R., Worringer, K. A., Wang, H., de la Cruz, C. C., Otte, A. P., Panning, B. and Zhang, Y. (2003). Role of histone H3 lysine 27 methylation in X inactivation. *Science* **300**, 131-135.
Saitou, M., Barton, S. C. and Surani, M. A. (2002). A molecular programme for the specification of germ cell fate in mice. *Nature* **418**, 293-300.
Sato, M., Kimura, T., Kurokawa, K., Fujita, Y., Abe, K., Masuhara, M., Yasunaga, T., Ryo, A., Yamamoto, M. and Nakano, T. (2002). Identification of PGC7, a new gene expressed specifically in preimplantation embryos and germ cells. *Mech. Dev.* **113**, 91-94.
Schaner, C. E. and Kelly, W. G. (2006). Germline chromatin (January 24, 2006). In *WormBook* (ed. The *C. elegans* Research Community), Wormbook, doi/10.1895/wormbook.1.73.1, http://www.wormbook.org.
Schaner, C. E., Deshpande, G., Schedl, P. D. and Kelly, W. G. (2003). A conserved chromatin architecture marks and maintains the restricted germ cell lineage in worms and flies. *Dev. Cell* **5**, 747-757.
Seki, Y., Hayashi, K., Itoh, K., Mizugaki, M., Saitou, M. and Matsui, Y. (2005). Extensive and orderly reprogramming of genome-wide chromatin modifications associated with specification and early development of germ cells in mice. *Dev. Biol.* **278**, 440-458.
Seydoux, G. and Dunn, M. A. (1997). Transcriptionally repressed germ cells lack a subpopulation of phosphorylated RNA polymerase II in early embryos of Caenorhabditis elegans and Drosophila melanogaster. *Development* **124**, 2191-2201.
Seydoux, G. and Braun, R. E. (2006). Pathway to totipotency: lessons from germ cells. *Cell* **127**, 891-904.
Silva, J., Mak, W., Zvetkova, I., Appanah, R., Nesterova, T. B., Webster, Z., Peters, A. H., Jenuwein, T., Otte, A. P. and Brockdorff, N. (2003). Establishment of histone h3 methylation on the inactive X chromosome requires transient recruitment of Eed-Enx1 polycomb group complexes. *Dev. Cell* **4**, 481-495.
Stewart, M. D., Sommerville, J. and Wong, J. (2006). Dynamic regulation of histone modifications in Xenopus oocytes through histone exchange. *Mol. Cell. Biol.* **26**, 6890-6901.
Su, T. T., Campbell, S. D. and O'Farrell, P. H. (1998). The cell cycle program in germ cells of the Drosophila embryo. *Dev. Biol.* **196**, 160-170.
Subramaniam, K. and Seydoux, G. (1999). nos-1 and nos-2, two genes related to Drosophila nanos, regulate primordial germ cell development and survival in Caenorhabditis elegans. *Development* **126**, 4861-4871.
Surani, M. A. (2001). Reprogramming of genome function through epigenetic inheritance. *Nature* **414**, 122-128.
Tachibana, M., Sugimoto, K., Nozaki, M., Ueda, J., Ohta, T., Ohki, M., Fukuda, M., Takeda, N., Niida, H., Kato, H. et al. (2002). G9a histone methyltransferase plays a dominant role in euchromatic histone H3 lysine 9 methylation and is essential for early embryogenesis. *Genes Dev.* **16**, 1779-1791.
Tachibana, M., Ueda, J., Fukuda, M., Takeda, N., Ohta, T., Iwanari, H., Sakihama, T., Kodama, T., Hamakubo, T. and Shinkai, Y. (2005). Histone methyltransferases G9a and GLP form heteromeric complexes and are both crucial for methylation of euchromatin at H3-K9. *Genes Dev.* **19**, 815-826.
Tam, P. P. and Snow, M. H. (1981). Proliferation and migration of primordial germ cells during compensatory growth in mouse embryos. *J. Embryol. Exp. Morphol.* **64**, 133-147.
Tsuda, M., Sasaoka, Y., Kiso, M., Abe, K., Haraguchi, S., Kobayashi, S. and Saga, Y. (2003). Conserved role of nanos proteins in germ cell development. *Science* **301**, 1239-1241.
Wang, C. and Lehmann, R. (1991). Nanos is the localized posterior determinant in Drosophila. *Cell* **66**, 637-647.
Yabuta, Y., Kurimoto, K., Ohinata, Y., Seki, Y. and Saitou, M. (2006). Gene expression dynamics during germline specification in mice identified by quantitative single-cell gene expression profiling. *Biol. Reprod.* **75**, 705-716.
Zhang, F., Barboric, M., Blackwell, T. K. and Peterlin, B. M. (2003). A model of repression: CTD analogs and PIE-1 inhibit transcriptional elongation by P-TEFb. *Genes Dev.* **17**, 748-758.

Table S1. Summary of the immunofluorescence analyses in this study

Transcriptional repression in migrating PGCs

Stage	H5-positive	Reporter-positive cells analyzed
EB (*n*=1)	56 (100%)	56
EHF (*n*=1)	82 (95.3%)	86
LHF	152 (62.3%)	244
E8.25	22 (23.4%)	94
E8.5	5 (4.9%)	103
E8.75	23 (7.9%)	293
E9.25	72 (39.3%)	183
E9.25	102 (79.7%)	128
E10.5	123 (100%)	123

Increase of PGC number during the course of development

Stage	PGC number	Transgenic lines analyzed
LS	34.7±4.8 (*n*=3)	*Blimp1*-mEGFP
EB	48±6.5 (*n*=3)	
LB	69±4.6 (*n*=4)	
EHF	89.4±3.7 (*n*=9)	
LHF	91.4±3.8 (*n*=5)	*stella*-EGFP
E8.25	110.8±6.8 (*n*=8)	
E8.5	116±4.4 (*n*=9)	
E8.75	139±11.5 (*n*=8)	
E9.0	157.4±14.5 (*n*=7)	
E9.25	192.4±35.8 (*n*=5)	
E9.5	237.2±19.2 (*n*=10)	
E9.75	435.4±19.2 (*n*=5)	
E10.5	1411.5±292.1 (*n*=8)	

Number and percentage of BrdU-positive PGCs at each stage

Stage	BrdU-positive	Reporter-positive cells analyzed
LS (*n*=1)	20 (47.6%)	42
EB/MB (*n*=5)	90 (35.2%)	256
EHF (*n*=3)	28 (16.3%)	172
E8.25	13 (10.3%)	126
E8.5	33 (16.5%)	200
E8.75	14 (13.7%)	102
E9.0	10 (10.2%)	90
E9.25	20 (25%)	80
E9.5	24 (24%)	100
E9.75	54 (56.3%)	96
E10.0	58 (43.6%)	133
E10.25	72 (51.4%)	140
E10.5	60 (49.6%)	121

Number and percentage of Cyclin B1-strong-positive PGCs at each stage

Stage	Cyclin B1-strong-positive	Reporter-positive cells analyzed
LB (*n*=2)	19 (23.5%)	81
EHF (*n*=2)	47 (23.8%)	198
E8.25	69 (70.4%)	98
E8.5	126 (79.7%)	158
E8.75	30 (85.7%)	35
E9.0	98 (80.3%)	122
E9.25	127 (79.9%)	159
E9.5	108 (73.5%)	147
E9.75	48 (42.1%)	114
E10.0	24 (29.3%)	82
E10.25	32 (32.7%)	98
E10.5	48 (42.9%)	112